The Cleanroom-Free, Cheap, and Rapid Fabrication of Nanoelectrodes with Low zM Limits of Detection

Gabriel Maroli, Vernalyn Abarintos, Andrew Piper,* and Arben Merkoçi*

Nanoscale electrodes have been a topic of intense research for many decades. Their enhanced sensitivities, born out of an improved signal-to-noise ratio as electrode dimensions decrease, make them ideal for the development of low-concentration analyte sensors. However, to date, nanoelectrode fabrication has typically required expensive equipment and exhaustive, time-consuming fabrication methods that have rendered them unsuitable for widespread use and commercialization. Herein, a method of nanoband electrode fabrication using low cost materials and equipment commonly found in research laboratories around the world is reported. The materials' cost to produce each nanoband is less than €0.01 and fabrication of a batch takes less than 1 h. The devices can be made of flexible plastics and their designs can be quickly and easily iterated. Facile methods of combining these nanobands into powerful devices, such as complete three-electrode systems, are also displayed. As a proof of concept, the electrodes are functionalized for the detection of a DNA sequence specific to SARS-CoV-2 and found to display single molecule sensitivity.

1. Introduction

For many years now, electrochemists have been limited by the choice of available electrodes. Traditional gold, silver, and carbon electrodes are routinely used around the world and can be purchased for a few hundred euros each. However, these electrodes require polishing by hand in alumina slurries, chemical cleaning in harsh, environmentally unfriendly solvents (such as piranha solution), sonication, and electrochemical cycling in strong acids (e.g., H_2SO_4), in order to clean them before use.[1–3] This is all done to try and get the electrodes as clean, flat, and reproducible as possible. The oldest alternative to these electrodes is the dropping mercury electrode,[4] where mercury is dropped through a small capillary to constantly create a fresh electrode surface of a defined area at which measurements can be taken. Due to safety concerns over working with mercury, these are rarely used nowadays.

More modern alternatives include inkjet and screen-printed electrodes.[5–8] In such electrodes, nano-/microparticle inks are patterned onto a substrate. To prevent aggregation, the nanoparticles need to be stabilized in solution by adding bulky organic ligands to make them stable colloids. The presence of these ligands can impede subsequent electrode performance and their removal post-printing is difficult given their size and covalent attachment to the nanoparticles. The printed electrodes are incredibly rough and irreproducible, which contributes to irreproducibility in the intended applications. In most cases, the devices are not conductive immediately after printing and need to be "sintered," a process by which the conductive particles morph to increase the contact area between them.[9,44] Printed electrodes can be purchased commercially for several euros per electrode, with the exact price depending on the electrode type.

Alternatively, electrodes can be made in clean rooms. These facilities are expensive to build and their maintenance and running costs are prohibitively expensive for many research and commercial applications. Inside the clean room, conductive materials can be deposited on substrates in a highly controlled fashion with sub-nanometer resolution using chemical or physical vapor deposition, atomic layer deposition (ALD), or electron beam evaporation (E-beam).[10,11] ALD is a surface-controlled and self-limiting method for depositing thin films from gaseous precursors. This self-limiting growth mechanism allows sub-nanometer-level control of film thickness with an excellent conformity.[12] With E-beam, an electron beam is focused onto a target metal under high vacuum, vaporizing the metal in a high vacuum chamber where it can be deposited in a uniform thin film on a chosen substrate.[13,14] The cost of these tools is in the range of hundreds of thousands of euros. Electrodes made by this method offer the best electrode purity and smoothness. Likewise, by fabricating in a cleanroom, photolithographic processes can be used to make a variety of electrode designs and architectures with incredibly high resolution.

G. Maroli, V. Abarintos, A. Piper, A. Merkoçi
Catalan Institute of Nanoscience and Nanotechnology (ICN2)
UAB Campus
Bellaterra, Barcelona 08193, Spain
E-mail: andrew.piper@icn2.cat; arben.merkoci@icn2.cat
G. Maroli
UIDI-CONICET Universidad Tecnológica Nacional
Buenos Aires C1041AAJ, Argentina

The ORCID identification number(s) for the author(s) of this article can be found under https://doi.org/10.1002/smll.202302136
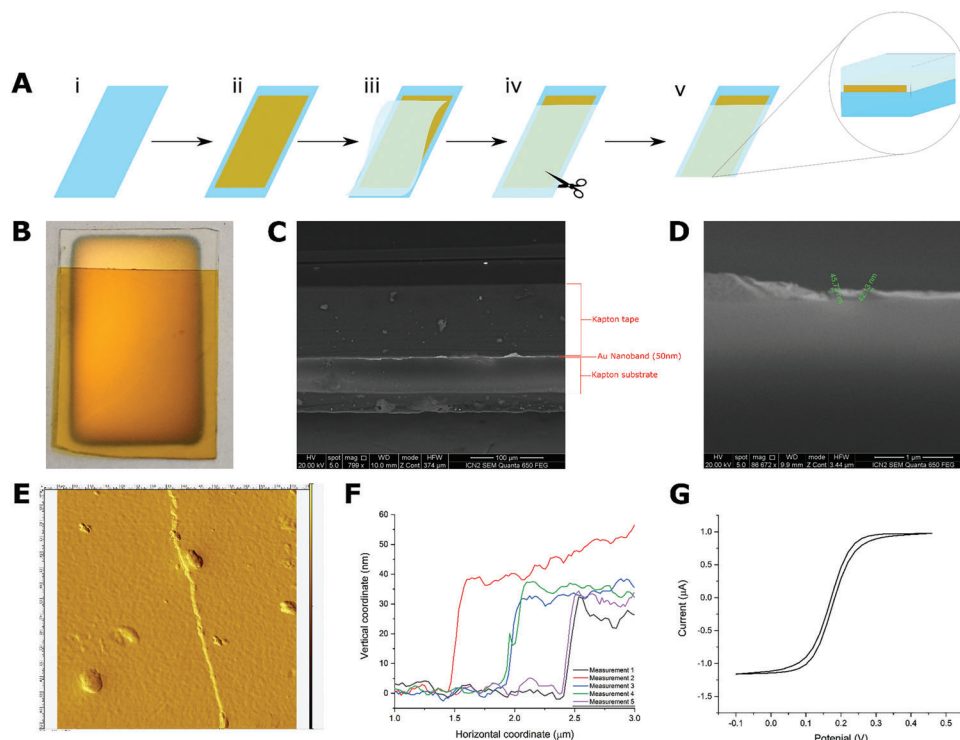
Figure 1. A) Schematic representation of the nanoband electrode fabrication showing i) the cleaned prepared substrate ii) after sputtering a nanometer thin layer of conductive electrode material through a mask iii) application of a capping layer iv) cutting to relieve a nanometer high edge electrode v) the completed device with a cross-section schematic (not to scale). B) Photograph of a device at step (iv), in this photograph the device was made with a PET substrate and Kapton tape capping layer. C,D) Scanning electron micrograph images of nanoband electrodes made with Au sputtered onto Kapton and capped with Kapton tape, cut with surgical grade scissors E) is an AFM image of the edge of one of the sputtered Au devices on Kapton (uncapped) with five corresponding step height measurements from left to right across the ridge in (F) showing that the Au thickness is $\approx$30–40 nm and the roughness of the Au surface is the same as the Kapton (single nanometers). G) CV of nanoband electrode, in 5×10^{-3} M potassium ferricyanide, 5×10^{-3} M potassium ferrocyanide, 100×10^{-3} M KNO$_3$ recorded at a scan rate of 10 mV s^{-1} versus a Ag/AgCl reference electrode and Pt wire counter electrode.

A nanoelectrode is defined as any electrode that has at least one of its dimensions on the nanoscale.[15,16] Nanoelectrodes have many advantages over conventional, macroscopic electrodes. Chief among which is their superior sensitivity.[17–20] This improvement in sensitivity as the electrodes get smaller can be attributed to three factors: The first comes from their enhanced mass transport, which allows them to measure a steady-state current; second, they have smaller double layers, which means that a greater proportion of the current is Faradaic; and finally, they have relatively smaller iR drops than larger electrodes.[17,20,21] Recent studies have also shown that nanoscale electrodes can be functionalized through the spontaneous formation of thiolate self-assembled monolayers (SAMs), the most common method of electrode functionalization, in a matter of seconds; rather than the hours taken to functionalize macroscale electrodes.[3] This means that sensor development and fabrication can be rapidly sped up if done on nanoscale electrodes. At the time of writing, nanoelectrodes are typically either made using complementary metal–oxide semiconductor fabrication techniques,[13,22] finely controlled chemical growth,[23] made in the form of nanowires[24,25] or grown on nanoscale templates.[26] These methods are either expensive or unsuitable for large-scale electrode manufacturing.

Here, we report a cleanroom-free method of nanoelectrode fabrication using sputter coaters. With this method, we are able to deposit metallic thin films with sub-nanometer resolution, outside of a cleanroom, using cheap equipment found in most research laboratories onto any substrate. These thin films are sandwiched between the substrate and a capping layer before being cut to relieve a nanoband electrode, see **Figure 1**. These electrodes are extremely cheap, with raw materials costing less than €0.10 per device, and can be cut multiple times in a matter of seconds to relieve brand new, pristine electrodes that require no cleaning prior to use. By cutting each device multiple times, the cost of each electrode can be reduced to below €0.01. We show that these electrodes possess the characteristic electrochemical properties of nanoelectrodes, including better signal-to-noise ratios and faster functionalization times than larger electrodes. As a proof of principle, we show the superior performance of these electrodes in the detection of DNA with the same sequence tested for in the quantitative reverse transcription polymerase chain reaction (PCR) diagnosis of SARS-CoV-2; where they exhibited superior sensitivities and limits of detection to conventional electrodes.

These electrodes are cheap, easy to fabricate, can be made in any lab in the world with commonplace, affordable equipment,

**ADVANCED
SCIENCE NEWS**

www.advancedsciencenews.com

**NANO · MICRO
small**

www.small-journal.com

are more sensitive than the commonly used electrodes, and can be functionalized to make sensors in minutes. They therefore have the potential to revolutionize any research that uses electrodes. They are superior in every way to electrodes made by other methods and have the potential to replace existing electrodes immediately, with little to no upfront capital costs. The faster functionalization times and lack of required cleaning means that assay development can be rapidly sped up on these electrodes. Finally, it is intended that the electrodes will allow more sensitive point of care sensors to be developed, allowing the diagnosis and prognosis of diseases with biomarkers too low in concentration for conventional sensors to detect, the earlier diagnosis of diseases (when the concentration of biomarkers is lower), and perhaps even the amplification-free detection of nucleic acid biomarkers.

2. Results and Discussion

2.1. Electrode Fabrication and Characterization

The nanoelectrodes in this project were fabricated by sputtering gold, using a conventional sputter coater, through a mask (stencil) onto various flexible plastic substrates. The substrates tested were polyimide (Kapton), polyethylene terephthalate (PET), and polyethylene naphthalate (PEN). These substrates were chosen because they are cheap, widely available, flexible, and easy to cut. The ability to form these electrodes on any vacuum stable substrate, without any optimization of the fabrication, is a major advantage of this work over alternative methods. The masks used in this project as stencils were made of aluminium or any of the aforementioned plastics, theoretically they can be made out of any material that does not interfere with the sputtering. The stencils are required to have sufficient weight to sit flush on the substrate and keep it in place during the evacuation of the sputter chamber. This is important to make electrodes reproducibly, as any lifting or deformation of the mask can change the sputtered electrode dimensions. The ability to rapidly design, cut, and use masks with different layouts allows a fast iterative approach for electrode design. This is not possible using photolithography where new masks take much longer to design and fabricate. In this study, a simple design motif of 1.2 cm wide and 2.4 cm long rectangles was used, Figure 1A,B and Figures S1 and S2 in the Supporting Information.

The rate of Au deposition by sputtering is well reported in the literature, and our measurements of the electrode thickness as a function of time and deposition current were found to be in agreement with other publications.[27,28] This method allows for the controlled deposition of nanometer thin metallic films with sub-nanometer precision; using cheap equipment that is routinely found in most laboratories around the world, since sputter coaters are used in scanning electron microscope (SEM) sample preparation. In this work, we sputtered metallic layers 50–100 nm thick. The rationale behind this was to make the devices thick enough to ensure a good connection through a crocodile clip on the bond pad, to ensure a homogenous coverage of the substrate and to have the same thicknesses as similar cleanroom-fabricated nanoelectrodes present in the literature.[3,17,18,27–29]

The deposited metal (in this case Au) was initially tested with a four-point probe to assess its conductivity. The mask allowed us to make five devices on each substrate, see Figure S2 in the Supporting Information, the sheet resistances of the sputtered metal films on different substrate have been provided in Table S1 in the Supporting Information, as well as that of E-beamed Au on Kapton, for reference. All the measured values are the same order of magnitude ($m\Omega\,sq^{-1}$) with the E-beamed Au having a sheet resistance about half that of the sputtered Au. There is no significant difference between the resistances of the gold sputtered onto any of the different substrates, this is pleasing as it evidences that the substrate does not affect the electrochemical performance of the devices.

In order to create nanoelectrodes, the sputtered metal needed to be "capped" and cut. Several capping methods were tested, including: covering with Kapton tape, spray coating with acrylic, and laminating with an office laminator. All were found to work, Figures S3–S6 in the Supporting Information, and may be suited to different applications. The requirements for a good capping layer are that it strongly adheres to both the electrode material and the substrate, is chemically inert in the media in which it will be tested, forms a good physical and dielectric barrier, and does not damage the underlying electrode. It should also be easy to cut with the intended cutting method. In this project, we favored using the Kapton tape because it was quicker to make devices with this than the other methods which need to be left to dry (acrylic) or heated (lamination).

Once the devices are capped, they must be cut to relieve nanoband electrodes. The cutting was performed with scissors, scalpels, or a paper guillotine, see Figure S4 in the Supporting Information, all were capable of producing nanoband electrodes. In order to make functioning electrodes, the blades in each of the cutting methods need to be as sharp and clean as possible (e.g., it is necessary to use surgical grade or microscopy scissors rather than office scissors). If the blade was blunt, it would cause a deformation of the layers, Figure S7 in the Supporting Information. Finally, the capping layers do not all set hard and should be cut face down to drag the adhesive away from the electrode, so as not to cover it.

Cyclic voltammograms (CVs) of each substrate type, with each capping layer and cutting method have been included in Figure S6 in the Supporting Information. It is clear from the wave-like shapes of the CVs and the low capacitances of the electrodes that they are all nanoelectrodes. From Figure S6 in the Supporting Information, the most reproducible cutting method was the precision cutter, followed by the scissors and finally the scalpel. This trend can be explained by the methods that allow for the most human error causing the most irreproducibility. When cutting with the scalpel, the angle, pressure, and straightness of the cut are more irreproducible than with the other cutting methods.

Regarding the capping layers, the acrylic is the most reproducible owing to the fact that it sets the hardest. The softer setting adhesives of the tape and melt layer of the laminate are prone to being smeared on the electrodes during cutting. This is why it is important to cut the electrodes in a fashion that drags the adhesive away from the electrode. Although some damage is still possible, which is why the precision cutter gave not only the most reproducible cuts, see Figure S6 in the Supporting Information, but also consistently yielded electrodes with a higher area; as there is less adhesive on the electrodes. Examples of the adhesive smearing can be seen in Figure S8 and the video in the Supporting

Information. In all experiments, the substrates tested had no discernible impact on the final electrode quality.

The time taken to make a single batch of electrodes, including sputtering, capping, and cutting was less than 1 h. Once the devices are made, fresh electrodes can be made by cutting in a matter of seconds. This is a crucial advancement over other cleanroom-free nanoelectrode fabrication methods such as those reported by the White group,[30] in which substrates are sputter coated through a mask and then encapsulated in resin which takes 24 h to dry, before being mechanically polished for hours to create pristine flat electrodes. A video showing the entire fabrication process has been made to accompany this publication. The equipment used is commonly found in most laboratories around the world but the up-front capital costs are also very low if they do need to be purchased. Table S2 in the Supporting Information summarizes these capital costs and the cost of consumables used for electrode fabrication. If the upfront equipment costs are excluded, then the materials' cost per electrode is below €0.01, on the condition that the devices are cut a minimum of ten times each, to yield at least ten electrodes per device. This makes these electrodes cheap and therefore inherently disposable, it is cheaper to cut and create a new electrode rather than trying to clean and re-use them. The ability to cut one device several times to make multiple electrodes is a novel advantage of these devices. The devices can take up to an hour to make but cutting and making a fresh nanoelectrode takes seconds.

To confirm that the fabricated electrodes are truly nano in nature, the bands were imaged by SEM, Figure 1C,D, the height of the uncapped sputtered metal edges was measured by atomic force microscopy (AFM), Figure 1E,F, and the nanoscale electrochemical responses of the bands were evaluated. The SEM images clearly show a nanoscale conductive band between the substrate and capping layer. Using the SEM software (xT microscope Control), the height of this band could be estimated and was found to be between 40 and 45 nm, which was slightly below the 50 nm targeted sputtering thickness of these devices. This slight variation is attributed to experimental errors in the sputtering since the AFM measurements of uncapped Au layers sputtered onto Kapton also had a step height of about 40 nm.

Typical CVs of macroelectrodes have peaks that form as the current becomes limited by the mass transport of the redox molecule to the electrode surface. The response of nanoelectrodes is different,[24,31] because the electrodes are so small, a hemispherical diffusion profile is rapidly established.[15,32] Therefore, waves rather than peaks are observed in the CVs of nanoscale electrodes.[33–35] The nanoband electrodes developed in this project exhibit electrochemical responses typical of nanoscale electrodes, Figure 1G. Likewise, the current ranges observed are in good agreement with nanobands of similar dimensions in similar buffers reported by other groups.[30] Another interesting electrochemical feature of the nanoelectrodes is the extremely low capacitances that they display, in this system the only capacitance present is the double layer capacitance (C_{dl}). The magnitude of the C_{dl} is given by the Helmholtz equation, Equation (1)[31]

$$C = \frac{\epsilon_0 \epsilon_r A}{H} \tag{1}$$

where C is the capacitance in Farads, ϵ_0 is the dielectric permittivity of a vacuum, ϵ_r is the dielectric permittivity of the measurement solution, A is the area of the electrode, and H is the separation distance between the plates in the model. In aqueous systems, H can be taken as the inner Helmholtz plane (the diameter of a water molecule in pure water).[31] It is possible to approximate the electrochemical surface area of the nanoband electrodes using Equation (1), since the C_{dl} follows the electrode surface very accurately and the other values can all be taken from the literature for pure water ($\epsilon_0 = 8.854 \times 10^{-12}$ F m^{-1}; $\epsilon_r = 78.3$; $H = 2.75$ Å).[31] In these experiments, 75 nm thick electrodes were sputtered, with a geometric electrode surface area of 9×10^{-4} mm^2. We calculated the area of our electrode, from its voltammetric capacitance, Figure S9 in the Supporting Information, to be $13.5 \times 10^{-4} \pm 0.6 \times 10^{-4}$ mm^2, within experimental error the same as the geometric area. These data further evidence the nanoscale nature of the electrodes. Likewise, the standard deviation was obtained from three electrodes cut on a single device, showing the reproducibility of the cutting method and the uniformity of the sputtered Au over the entire device. The slightly larger electrochemical surface area than geometric surface area is attributed to surface roughness and heterogeneity.[36] It is satisfying that our so-called "roughness factor" is 1.5, which is better than reported for other electrode types in the literature.[37] In this system, we postulate that as the capping layer adhesive is setting, it may move (during handling), dragging the Au layer out of the device, much like the filling in a sandwich when it is pressed. This theory is based on the SEM data, Figure 1D, where films appear to protrude from the device. This is further supported by the findings that the signals from the hardest setting capping layers (acrylic) gave the most reproducible electrodes. Also, anecdotally, the electrode reproducibility could be improved by leaving any of the capping layer types for extended periods of time (days/weeks depending on the capping material), to allow them to set harder.

To further characterize the electrochemical response of the nanobands, they were analyzed by electrochemical impedance spectroscopy. The Nyquist plot from these experiments has been provided in Figure S12 in the Supporting Information, within an inset showing the equivalent circuit to which it has been fit. This is the established equivalent circuit for nanoelectrodes.[3,15,35] The fitted values of the fit, reported in Table S5 in the Supporting Information, include an R_{ct} of 29 980 Ω ± 3.5% (error from the fitting). This was used to determine an electron transfer rate of 8.03 cm s^{-1}, the derivation of which is included in Figure S13 in the Supporting Information, which is in agreement with other nanoelectrodes in the literature.[32,35,38]

2.2. Different Electrode Designs

One of the advantages of making electrodes using this methodology is the ability to rapidly iterate different electrode designs and configurations. New plastic masks can be made quickly (in under 20 min) and easily using cutting plotters (or by hand) to change the pattern and size of the metallic coatings to suit different applications. Likewise, it is very easy to combine electrodes of different designs and types to create customized devices for different applications. It is easy to fabricate a library of electrodes of different patterns and thicknesses, sputtered from different materials.
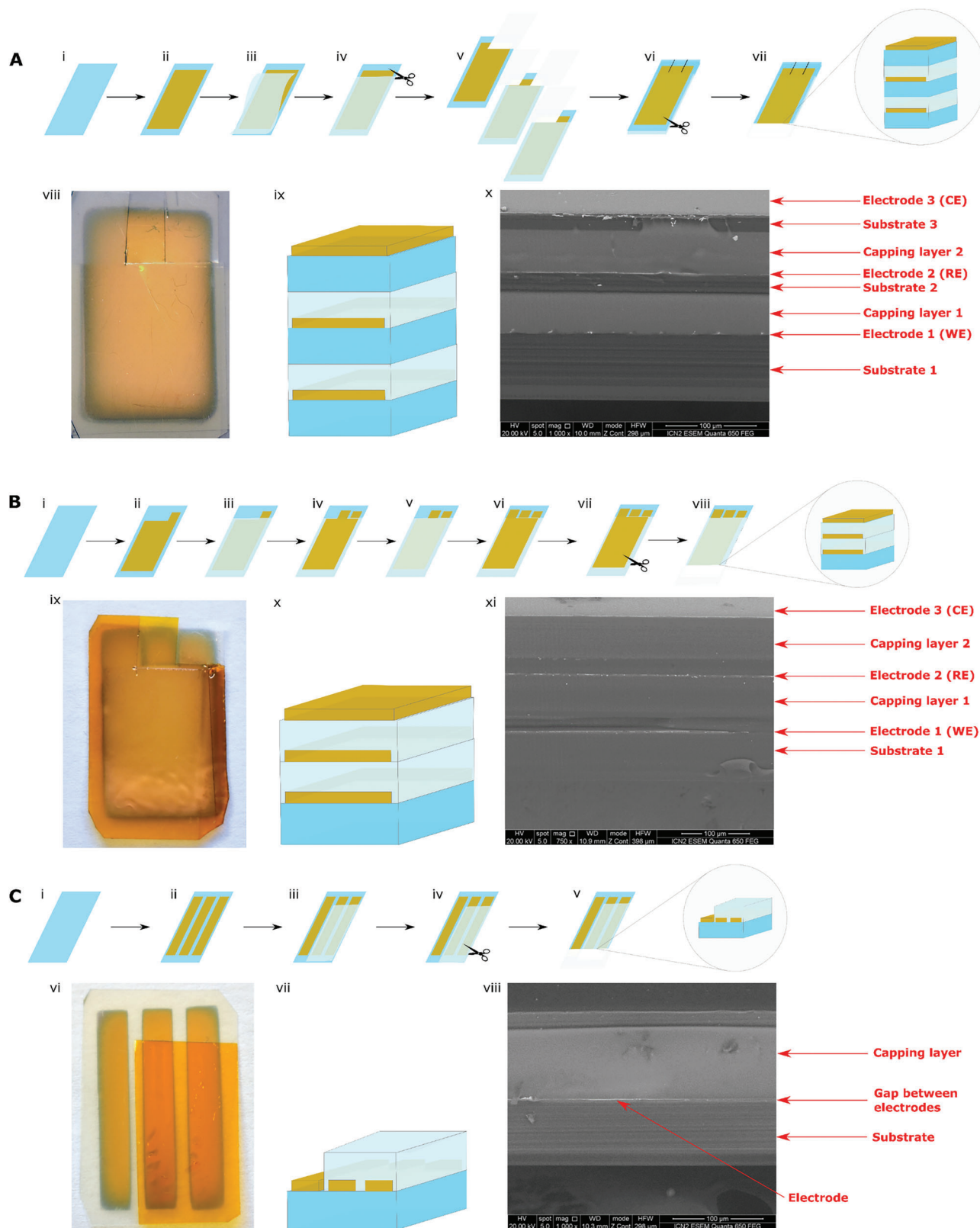
Figure 2. Schematics (not to scale), photographs, and SEM images of the different LEGO brick designs fabricated and tested in this project. A) Sticking completed devices on top of each other: i) a cleaned substrate, ii) is sputter coated with a nanometer thin film of Au, iii) before being capped, and iv) the bond pads cut so that each will open to the environment in the final 3D device, v) multiple separate devices are stacked and stuck to each other, vi,viii) before the three nanobands are exposed by cutting. viii) A photograph of one such completed device, ix) as well as a schematic and x) SEM of the

**ADVANCED
SCIENCE NEWS**

www.advancedsciencenews.com

NANO · MICRO

small

www.small-journal.com

These individual components can then be easily combined to develop new devices for different applications, including those with different numbers of electrodes, such as two-electrode systems or for multiplexed sensing applications. Much like LEGO bricks, these can be attached together to create an endless possibility of designs. As a proof of principle for this "LEGO-brick" concept, complete three-electrode systems have been developed by a number of different methods. The authors would like to stress that this is simply a proof of concept and that an endless number of designs are possible. Photographs, schematics, and SEMs of these different methods of combining devices have been shown in **Figure 2**. First, it is possible to stick multiple capped devices on top of each other using adhesives, see Figure 2A. Second, it is possible to build the devices up vertically by sputtering directly onto the capping layers, using masks to separate the different bond pads for the different layers, Figure 2B. Third, it is possible to design a mask in which the three electrodes are in the same 2D plane and simply separated from each other by the mask design, Figure 2C. The CVs of these devices, Figure S10 in the Supporting Information, show that there is a shift in the half-wave potential (from +0.175 to +0 V) when switching from a Ag/AgCl reference electrode to a sputtered Au pseudoreference electrode, as would be expected. Other than this, there is no difference in the obtained electrochemical signal, proving that functioning complete three-electrode systems can be produced by this "Lego-brick" method.
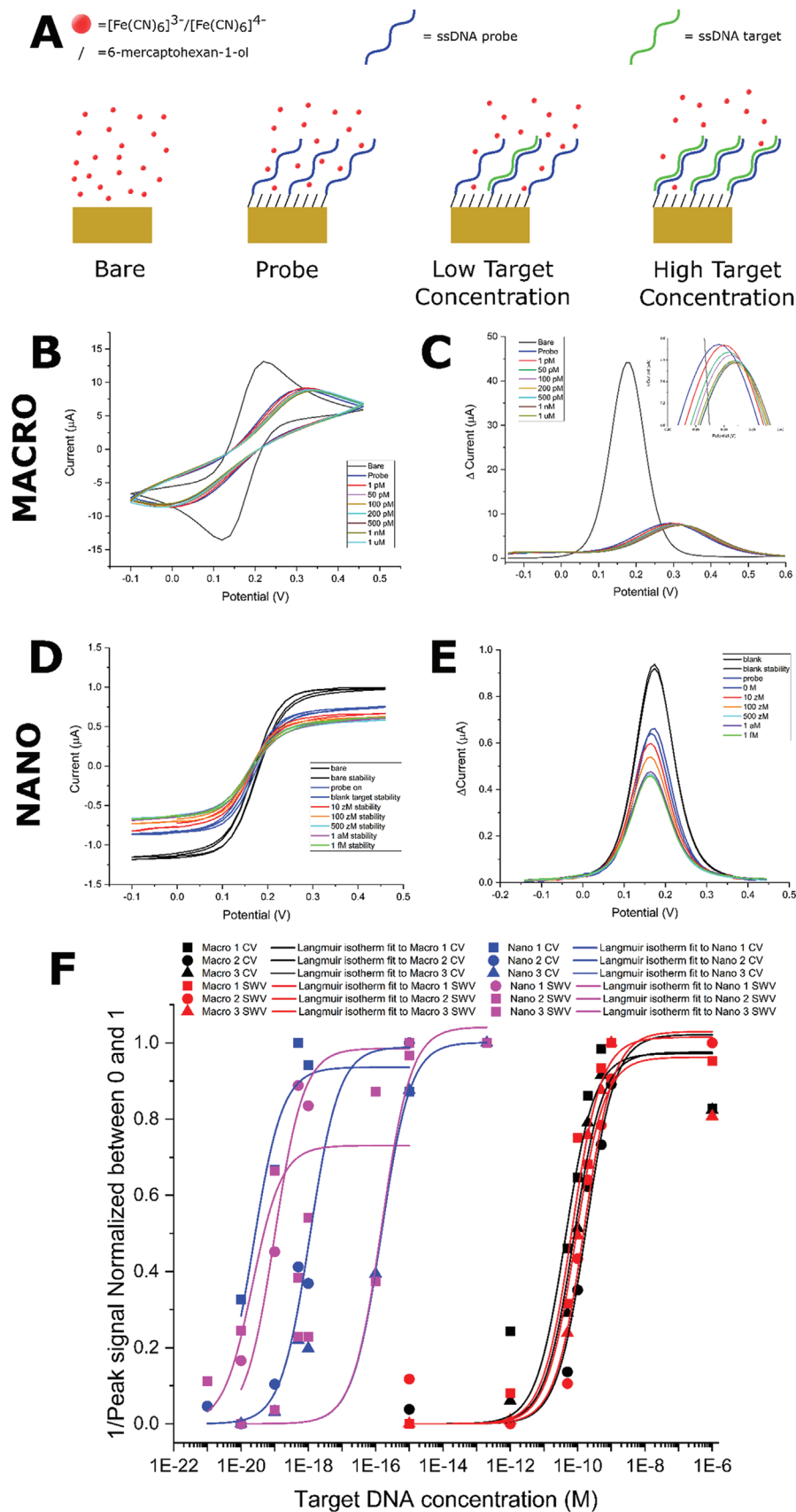
2.3. DNA Detection

In order to assess the sensing performance of the **e**lectrodes, they were functionalized with an ssDNA probe for the detection of a DNA sequence specific to SARS-CoV-2. The authors would like to stress that this is a proof-of-concept experiment, intended to ascertain the performance of the nanoband electrodes and compare them to existing commercial electrodes. As such, it was deemed suitable to detect a synthetic complimentary DNA sequence rather than RNA from real samples and the authors wish to stress that no claims are being made that an amplification-free SARS-CoV-2 sensor has been developed. The mode of operation of the sensor is shown schematically in **Figure 3**. First, the electrochemical response of a clean (bare) electrode is measured in a solution of 5×10^{-3} M $K[Fe(CN)_6]^{3-}$ and 5×10^{-3} M $K[Fe(CN)_6]^{4-}$ in $1 \times$ phosphate-buffered saline (PBS) with 10×10^{-3} M $MgCl_2$. Next, the electrodes were functionalized by the spontaneous formation of a mixed self-assembling monolayer from an aqueous solution containing 6-mercaptohexan-1-ol and a thiol-C6-modified ssDNA probe. This process takes a minimum of 2 h on macroscopic electrodes but was possible in less than 2 min on the nanoband electrodes. This is in agreement with previous publications and further evidences the nanoscale properties of these electrodes.[3] When placed back in the redox agent-containing solution and the electrochemistry was re-measured,

there is a clear decrease in the limiting current, Figure 3. This is because the charge transfer at the electrode is impeded by the steric blocking of the redox molecules by the SAM film, as well as the electrostatic repulsion of the anionic Fe species by the negatively charged phosphate backbone of the DNA. A control experiment was run to assess the stability of the SAM over the timescale of an assay, Figure S11 in the Supporting Information, in this control experiment, the functionalized nanobands were dipped into solutions of DNA-free water. In the main experiment, the functionalized electrodes were first placed in a solution of deionized water and then left to sit in the measurement solution for 20 min to make sure the probe monolayer was also stable. After which, it was placed consecutively in solutions containing increasing concentrations of target DNA before being rinsed with, and measured in, the measurement solution. The washing was important to remove any nonspecifically bound DNA from the surface. As the target DNA sequence binds to the probe layer, it further impedes the charge transfer at the electrode surface causing a decrease in current that is proportional to the amount of target DNA bound to the surface.

The CV and square wave voltammetry data from these experiments on macro and nanoband electrodes are provided in Figure 3. The Langmuir isotherm was chosen as the simplest and most appropriate model to fit these data to and from the fits, the technical limit of detection (LoD) of the macroelectrodes was found to be $92.4 \times 10^{-12} \pm 30.4 \times 10^{-12}$ M. However, the performance of the nanoband electrodes is significantly different, showing a clear sensitivity enhancement with a LoD of $97.1 \times 10^{-21} \pm 23.7 \times 10^{-21}$ m (1 zM = $\times 10^{-21}$ M) obtained in one of the repeats. While these limits of detection are very low, there is evidence in the literature of other nanoelectrode and nanoelectrode ensembles exhibiting similar sensitivities, including for DNA detection.[39–42] Avogadro's number is 6.022×10^{23}, meaning that a 10×10^{-21} m solution will contain 6000 molecules per liter. Therefore, a 2 mL solution of target DNA (as was being used here) should theoretically contain 12 target DNA strands. This means that with an LoD of 97×10^{-21} m, as few as 117 molecules in the 2 mL sample can be detected. However, the authors would emphasize caution on this front, these target DNA concentrations were made up by serial dilutions and there is obviously an error introduced by the pipetting. Table S4 in the Supporting Information shows the error in the final DNA concentration when different pipetting errors are taken into account. Even a 1% error (which is low for even the best of pipettes) could result in significantly more (or less) DNA in the low target DNA concentrations than is quoted here. Therefore, the authors would like to emphasize that the sensitivity of these electrodes is thought to be in the low zM range, based on these data and are not claiming single molecule detection limits. There are also concerns about whether or not 20 min is sufficient for such low amounts of analyte to diffuse to the electrode surface and bind to

---

cross-section have also been provided. B) Sputtering directly onto the capping layers. i) A cleaned substrate, ii) is sputter coated with a nanometer thin Au coating through a mask that also patterns the contact pad, iii) it is then capped, iv–vi) before sputtering and capping are repeated, using different masks to separate the contact pads, vii) the devices are then cut to relieve the nanobands. It is possible to leave the top layer uncapped so when dipped in solution its area is much larger than the other electrodes, allowing it to be used as a counter electrode. ix) A photograph and x) cross-sectional schematics and xi) an SEM image of this type of device. C) 2D devices. i) A cleaned substrate is sputter coated ii) with Au through a mask that patterns separate devices on the substrate surface. These can then be iii) capped and iv) cut to relieve multiple electrodes with variable shapes and orientations in the same plane. v) Photographs and vi) cross-sectional schematics and vii) SEMs have been provided.

ADVANCED
SCIENCE NEWS

www.advancedsciencenews.com

NANO · MICRO
small
www.small-journal.com

2302136 (7 of 11)

**ADVANCED
SCIENCE NEWS**

www.advancedsciencenews.com

NANO · MICRO

small

www.small-journal.com

the probes. We propose that bulk solution movements, such as convection and the agitation of the solution when the electrodes are inserted by hand, account for there being a sufficient amount of probe target hybridization in the 20 min tested.

What is clear, however, is that the sensitivity of these nanoband electrodes is far superior to that of the macroelectrodes and comparable to the best results for nanoelectrodes reported in the literature.[40] The variation in the nanoelectrode signal, at first glance, appears to be greater than that of the macroelectrodes. However, it should be noted that the *x*-axis is logarithmic, and the pipetting errors are larger for the lower analyte concentrations, therefore the spread of the data cannot be solely attributed to variation in the electrodes which were previously shown to be very reproducible. The difficulty in reproducibly making the calibration solutions with such low concentrations means that it is not possible to obtain linear ranges from the data shown in Figure 3F. The only conclusions that can be drawn are that these nanoband electrodes are extremely sensitive, capable of detecting DNA down at low zM levels. Until methods of reproducibly making solutions with such low concentrations of analyte are developed, accurate calibration curves will be impossible to obtain.

3. Conclusions

Herein, we have reported the cleanroom-free fabrication of nanoband electrodes. The nanoscale nature of the electrodes has been proven electrochemically as well as by SEM and AFM. These devices are extremely cheap, with raw materials' cost of €0.01 per electrode and can be made immediately in most labs around the world using commonplace, low-cost equipment. The electrodes exhibit superior performance compared to conventional electrodes, not just in terms of cost, but they are easy to manufacture in customizable design motifs, require no cleaning, can be made out of a wide range of materials, and are extremely sensitive. In the proof-of-principle DNA sensor shown here, the nanoband electrodes were able to achieve low zM levels of detection; markedly better than the pM detection limits of the same system on a macroscopic electrode. We believe that given these advantages, this work and these electrodes have the potential to revolutionize the fields of electrochemistry and point-of-care sensing. The low LoDs of these devices means that they can be used to develop sensors for biomarkers present in samples at very low concentrations. Methods of making the electrodes suitable for real world sample analysis, such as microfluidics and antifouling strategies will be the focus of future work.

For decades now, commercial point-of-care biosensors have been limited to the detection of highly abundant biomarkers such as glucose, lactate, progesterone, and virions. It is hoped that the lower LODs of these cheap nanoband electrodes will kick start the development of biosensors for a wide range of low-concentration biomarkers. This could not only lead to the earlier diagnosis of diseases, when the biomarkers are less abundant, but also to the development of point-of-care devices for disease states with

biomarkers too dilute to currently detect. This could include, but is not limited to, biomarkers that cross the blood brain barrier or cross the placenta from a fetal to a mother's bloodstream. Likewise, as has been shown by the detection of DNA here, it may be possible to replace PCR tests with amplification-free DNA sensors using this technology.

4. Experimental Section

Materials and Equipment: A Mini Sputter Coater (model SC7620, Quorum Technologies) and the gold sputter target were purchased from ANAME Instrumentación Científica (Madrid, Spain). The three substrates used were PET (thickness 75 µm), PEN (thickness 125 µm), and Dupont grade Kapton HN (thickness 75 µm), all were purchased from Goodfellow GmbH (Spain). The capping layers were 3 M Kapton tape 5413 (Digi-Key), Acrylic Varnish CRC – Clear Brilliant (RS Components Spain), and Fellowes Enhance 80 micron lamination sheets (Amazon, Spain). The cutting was performed with a flintronic A4 Paper Cutter (Amazon, Spain), scalpels, or surgical scissors purchased from VWR, Spain. Aluminum masks were made in house. A Graphtec ce6000-40 cutting plotter was used to fabricate masks out of the aforementioned Kapton that was also used as a substrate.

Potassium hexacyanoferrate (III) ($K_3[Fe(CN)_6]$) and potassium hexacyanoferrate (II) 3-hydrate ($K4[Fe(CN)6]\cdot 3H_2O$) were purchased from Panreac AppliChem. Tris(2-carboxyethyl)phosphine (TCEP), 2-mercaptohexanol, 2-propanol (IPA), acetone, and PBS, potassium nitrate (KNO_3), and magnesium chloride ($MgCl_2$) were purchased from Merck KGaA, Germany. Gold working electrodes (CH101), Ag/AgCl reference electrodes (CH111), and platinum wire counter electrodes (CH115) were purchased from CH instruments. Au/Au/Au screen-printed electrodes were purchased from DropSense, Spain. The 0.3 µm alumina low viscosity polishing slurry (ET034), 0.05 µm alumina low viscosity polishing slurry (ET033), micropolishing cloths (ET032), and glass polishing slides (ET031) were purchased from eDAQ (Poland). Concentrated sulfuric acid (96%, ITW, Spain) and hydrogen peroxide 50% (Sigma Aldrich, Spain) were used to make piranha solution for electrode cleaning. An Ovan Ultrasonic 3L bath was purchased from Ovan (Spain). All aqueous solutions were prepared using deionized water from a Milli-Q Advantage A10 Water Purification System with 0.22 µm filters MPGP04001 (18.2 MΩ cm, Merck-Millipore, Spain). The electrochemical measurements were carried out with a Metrohm Autolab PGSTAT12 with NOVA 2.1 software. All the data analysis was performed in the NOVA 2.1 software or Origin 2018, unless stated otherwise.

Nanoelectrode Fabrication—Sputtering: The chosen substrate (Kapton, PEN or PET) was cut into 6 cm x 6 cm squares with the cutting plotter. These dimensions were chosen to fit underneath the mask and inside the sputter coater. The mask pattern was created using AutoCAD software, version 2021 from Autodesk. The design was created with 0 mm strokes to generate a vector file. The Kapton masks were produced using a Graphtec ce6000-40 plotter, while the aluminum masks were machined using a Haas vf 1 CNC milling machine. The substrate was cleaned by soaking in acetone for 5 min, rinsed under a stream of IPA to remove the acetone before being completely immersed in a bath of IPA for another 5 min. Finally, the substrate was rinsed with ultrapure water. Note, poor cleaning can affect the adhesion of the sputtered metal to the substrate. The cleaned substrate and the mask were placed in the sputter coater with a preloaded Au sputter target. Vacuum was applied until a pressure <0.8 mbar was achieved. The chamber was flushed three times with Ar to remove any remaining oxygen. The Ar inlet was opened and a

Figure 3. A) Schematic illustration of how the DNA sensing mechanism works. B) Overlayed CVs of the DNA sensing system response to different target DNA concentrations on a macroelectrode. Overlayed with Square Wave Voltammetry (SWV) data from the experiments, shown in (C). The results of the same experiment, with lower DNA target concentrations on nanoband electrodes are shown in (D) and (E). The conditions for these experiments are set out in detail in the experimental section. F) The calibration curves from the macro and nanoelectrode repeats with corresponding fits to the Langmuir isotherm. The reciprocal of the peak signal was normalized between 0 and 1 prior to plotting and fitting.

**ADVANCED
SCIENCE NEWS**

www.advancedsciencenews.com

NANO · MICRO

small

www.small-journal.com

potential was applied to create the argon plasma and begin sputtering. By controlling the gas pressure in the chamber (with the inlet valve), the current could be altered, which determined the target metal deposition rate. In this project, a 10 mA current was chosen and a deposition rate of 5 nm min^{-1} was produced. The duration of the sputtering could then be used with this deposition rate to make devices any desired thickness. Once the sputtering process was finished, the chamber was vented and the substrate was removed, see the Supporting Information video.

Capping—Adhesive tape: The freshly sputtered device was fixed onto a flat surface. The tape was aligned and a small portion was stuck to the work surface to aid the alignment. The tape was then dragged across the surface of the device by hand, under constant pressure to avoid the formation of bubbles. The excess tape was removed and the devices were taken onto the next step.

Spray Coating: The device was fixed onto a flat surface. A plastic mask was used to define the area to be spray coated. The spray coating (in this project acrylic) was applied as per the manufacturer's instructions, by shaking vigorously before use and spraying from 20 cm above the device. The spray coating was repeated thrice to ensure a complete covering of the devices before they were left to dry under ambient conditions for 20 min prior to use.

Lamination: The freshly sputtered devices were placed on a sheet of paper. A pre-patterned lamination sheet (PET, with an ethylene vinyl acetate, EVA, inner coating) with pieces was cut out to leave exposed contact pads on the finished devices, was aligned and placed onto the devices. The ensemble was then run through a Lamigator IQ (Renz, Spain), to laminate the devices in a hot lamination process where EVA acted as a melt adhesive.

Cutting: The different cutting methods investigated in this project were to cut with a scalpel, scissors, and a flintronic A4 paper cutter. The blades of each device were rinsed with IPA and dried with N_2 prior to each cut. After repeated use, the blades could get blunt and either needed to be replaced or sharpened. It is vital to have the capping layers facing away from the direction of travel of the blade to avoid any adhesive being dragged over the working area of the nanoband being created.

Scalpel Cutting: The devices were fixed face down (with tape) on a Model craft cutting mat (RS components, Spain). A clean scalpel was used to cut the devices by hand by applying as even and uniform a pressure as possible with the blade perpendicular to the mat in a single swift stroke using the markings on the cutting mat to guide the alignment of the cut.

Scissor Cutting: Microscopy (surgical) grade scissors were needed as conventional office scissors are not sharp enough for this application. The devices were placed face down with the region that was intended to be cut resting on the bottom blade of the scissors. The upper blade was closed quickly and smoothly keeping it as perpendicular to the device as possible.

Flintronic Paper Cutter: The devices were stuck face down on the cutter surface, using the alignment markings on the surface to ensure the blade was cutting as straight across the device as possible. The blade was pushed down and dragged through the device at a uniform speed and pressure. In this instance, it was held perpendicular to the device by the design of the tool.

Sheet Resistance of the Metals: The sheet resistances of the Au sputtered onto different substrates were measured using a Keithley DMM6500 multimeter in a 4-point probe mode. Pogo pins with a pressure of 120 g and a separation of 2.54 mm were used. As is required for determining the sheet resistance of thin layers, a correction factor of 4.53 and a geometric correction factor of 0.78 were used when performing these experiments.[43]

The e-beamed samples used as a control were sputtered onto a 4″ Kapton substrate using the same mask as was used in the sputter coater. 35 nm of Au was deposited through the mask onto the substrate using an ATC-8E Orion evaporator (AJA International Inc., USA).

AFM and SEM: The samples were mounted on SEM sample stubs using double sided conductive carbon tape (TED Pella, INC), these were then loaded into a Thermo Fisher (formerly FEI) Quanta 650 FEG ESEM for image acquisition using the backscatter electrons detector under low vacuum conditions. In all the figures presented, the electron beam intensity, working distance, and magnification were stated.

AFM images were obtained through Molecular Imaging's PicoPlus modular Scanning Probe Microscope (SPM) system in combination with the PicoScan Controller and magnetic MAC Mode. PicoView 1.20 software was used during data acquisition but the analysis and corrections were performed in Gwyddion 2.61.

Electrochemical Characterization: The electrodes were characterized by CV, square wave voltammetry, and electrochemical impedance spectroscopy. Unless stated otherwise, the bare electrodes were tested in solutions of 5×10^{-3} M potassium ferricyanide, 5×10^{-3} M potassium ferrocyanide, and 1x PBS versus a silver/silver chloride reference electrode and Pt wire counter electrode. CVs were run between −0.1 and + 0.45 V at a scan rate of 10 mV s^{-1}, for a total of four cycles. The square wave voltammetry was run in the same set up immediately after the CVs from −0.15 to +0.6 V versus the open circuit potential with a 9 mV step, a modulation amplitude of 20 mV, and a frequency of 2.5 Hz. The electrochemical impedance spectroscopy was run with a dc voltage equal to the measured open circuit potential, with a 10 mV sinusoidal AC voltage over a frequency range of 100 kHz to 0.1 Hz, recording 10 frequencies spread logarithmically per decade.

DNA Sensing: The DNA probe was a thiol tagged primer approved by the Centre for Disease Control (CDC) for the detection of SARS-CoV-2. The sequences were ordered from Merck (Spain) and were as follows:

Probe 5´- ACCCCGCATTACGTTTGGTGGACC-(C_6SH) - 3'
Target 5´- GGTCCACCAAACGTAATGCGGGGT - 3'

The electrodes were placed in an aqueous solution containing 30×10^{-6} M 6-mercaptohexanol (MCH), 150×10^{-6} M TCEP, and 1.5×10^{-6} M of the probe DNA. The macroelectrodes were left in this solution for the self-assembled monolayer to form for 2 h, whereas the nanoelectrodes were left for 2 min, prior to rinsing with a stream of water to remove physisorbed thiols.

Before and after probe film formation, the electrodes were placed in a solution of 1x PBS with 10×10^{-3} M MgCl$_2$, 5×10^{-3} M potassium hexacyanoferrate (III) and 5×10^{-3} M potassium hexacyanoferrate (II). CVs were run between −0.1 and + 0.45 V versus a Ag/AgCl reference electrode (macro) or Au pseudoreference electrode (nano) and Pt wire counter electrode, at a scan rate of 10 mV s^{-1}, for a total of four cycles. The square wave voltammetry was run in the same set up immediately after the CVs from −0.15 to +0.6 V versus the open circuit potential with a 9 mV step, a modulation amplitude of 20 mV, and a frequency of 2.5 Hz.

After the probe film was formed the functionalized electrodes were placed in solutions containing increasing concentrations of DNA target, for 20 min each. Between target incubations, the electrodes were placed in the measurement solution, left for 20 min, and the electrochemical measurements were repeated. The DNA target concentrations tested were differed for the macro and nanoelectrodes. For the macroelectrodes, the target DNA concentrations tested were: 0 M, 1×10^{-15}, 1×10^{-12}, 500×10^{-12}, 1×10^{-9}, 500×10^{-9}, and 1×10^{-6} M. For the nanoelectrodes, the target concentrations tested were 0 M, 10×10^{-21}, 100×10^{-21}, 500×10^{-21}, 1×10^{-18}, and 1×10^{-15} M.

A control experiment was run where the functionalized nanoelectrodes were placed in MQ water rather than the increasing DNA concentrations, for the same number of repeats. A second control was run where the functionalized electrodes were exposed to noncomplimentary DNA target sequences.

Lego-Brick Concept: The different fabrication methods for the different 2D stacking designs (Lego brick) assemblies of the nanoband electrodes are described below. In all these cases, the substrate cleaning, sputtering, and capping were performed as described above.

2D Design: A mask was made out of Kapton, see Figure S2B in the Supporting Information, in which three electrodes could be patterned on a single device, running parallel to one another down the length of the device. The three electrodes were able to be used as a working electrode, pseudoreference electrode, and counter electrode. In the mask shown in Figure S2B in the Supporting Information, the electrodes were designed to be the same size, 3 mm wide and 21 mm long with 1.5 mm separations between them.

**ADVANCED
SCIENCE NEWS**

www.advancedsciencenews.com

**NANO · MICRO
small**

www.small-journal.com

Lego-Brick Concept 1: In this method, the individual devices were capped with the acrylic spray. Multiple devices could be stacked on top of each other with the acrylic acting as an adhesive between them. In this system, each of the devices performed the function of a working, counter, or reference electrode. In these experiments, the acrylic was needed to be left for longer to dry (overnight) under ambient conditions. The connection pads of each device could be cut with scissors to allow easy connection after stacking.

Lego-Brick Concept 2: In this method, new electrodes were sputtered directly onto the capping layer of the underlying device. Three mask designs (Figure S2C, Supporting Information) were used, one for each layer. The masks were designed to isolate the connections of each layer in the final device. The final layer, sputtered to be the counter electrode, was not capped, so that when dipped into a solution, the electrode area would be far greater than that of the working electrode.

Supporting Information

Supporting Information is available from the Wiley Online Library or from the author.

Acknowledgements

Conflict of Interest

The authors have no competing interests to declare.

Author Contributions

G.M. and V.A. contributed equally to this work. G.M. and V.A. contributed equally to the acquisition and analysis of the data as well as the paper writing. A.P. conceived the original idea, supervised the acquisition of the data, acquired the data, analyzed the data, wrote the manuscript, and led the project throughout. A.M. supervised the project and contributed to drafting the paper.

Data Availability Statement

The data that support the findings of this study are available from the corresponding author upon reasonable request.

Keywords

[1] G. Henihan, H. Schulze, D. K. Corrigan, G. Giraud, J. G. Terry, A. Hardie, C. J. Campbell, A. J. Walton, J. Crain, R. Pethig, K. E. Templeton, A. R. Mount, T. T. Bachmann, *Biosens. Bioelectron.* **2016**, *81*, 487.

[2] D. K. Corrigan, H. Schulze, G. Henihan, A. Hardie, I. Ciani, G. Giraud, J. G. Terry, A. J. Walton, R. Pethig, P. Ghazal, J. Crain, C. J. Campbell, K. E. Templeton, A. R. Mount, T. T. Bachmann, *Analyst* **2013**, *138*, 6997.

[3] A. Piper, D. K. Corrigan, A. R. Mount, *Electrochem. Sci. Adv.* **2021**, *2*, e2100077.

[4] A. Frumkin, A. Donde, *Z. Phys. Chem.* **1926**, *123*, 339.

[5] K. Kuribayashi, H. Matsumoto, Y. Uda, Y. Komatsu, A. Nakano, S. Ikegami, *Jpn. J. Appl. Phys., Part 1* **1983**, *22*, 1828.

[6] D. Mandler, S. Kraus-Ophir, *J. Solid State Electrochem.* **2011**, *15*, 1535.

[7] D. H. Craston, C. P. Jones, D. E. Williams, N. Elmurr, *Talanta* **1991**, *38*, 17.

[8] N. Komuro, S. Takaki, K. Suzuki, D. Citterio, *Anal. Bioanal. Chem.* **2013**, *405*, 5785.

[9] Y. Sui, C. A. Zorman, *J. Electrochem. Soc.* **2020**, *167*, 037571.

[10] N. M. Hemed, A. Convertino, Y. Shacham-Diamand, *Sens. Actuators, B* **2018**, *259*, 809.

[11] R. K. Gupta, A. Periyakaruppan, M. Meyyappan, J. E. Koehne, *Biosens. Bioelectron.* **2014**, *59*, 112.

[12] B. C. Mallick, C. T. Hsieh, K. M. Yin, Y. A. Gandomi, K. T. Huang, *ECS J. Solid State Sci. Technol.* **2019**, *8*, N55.

[13] D. E. Presnov, I. V. Bozhev, A. V. Miakonkikh, S. G. Simakin, A. S. Trifonov, V. A. Krupenin, *J. Appl. Phys.* **2018**, *123*, 054503.

[14] N. Elfstrom, R. Juhasz, I. Sychugov, T. Engfeldt, A. E. Karlstrom, J. Linnros, *Nano Lett.* **2007**, *7*, 2608.

[15] A. Piper, A. Mount, *Electrochemical Characterisation of Microsquare Nanoband Edge Electrode (MNEE) Arrays and Their Use as Biosensors*, University of Edinburgh, Edinburgh **2017**.

[16] I. Kleps, A. Angelescu, R. Vasilco, D. Dascalu, *Biomed. Microdevices* **2001**, *3*, 29.

[17] A. Piper, B. Alston, D. Adams, A. R. Mount, *Faraday Discuss.* **2018**, *201*, 201.

[18] E. J. F. Dickinson, R. G. Compton, *J. Electroanal. Chem.* **2011**, *661*, 198.

[19] M. Silvestrini, L. Fruk, P. Ugo, *Biosens. Bioelectron.* **2013**, *40*, 265.

[20] H. L. Woodvine, D. A. R. Mount, *Development and Characterisation of Microelectrode and Nanoelectrode Systems*, The University of Edinburgh, Edinburgh **2011**.

[21] J. G. Terry, I. Schmueser, I. Underwood, D. K. Corrigan, N. J. Freeman, A. S. Bunting, A. R. Mount, A. J. Walton, *IET Nanobiotechnol.* **2013**, *7*, 125.

[22] N. Couniot, T. Vanzieleghem, J. Rasson, N. Van Overstraeten-Schlogel, O. Poncelet, J. Mahillon, L. A. Francis, D. Flandre, *Biosens. Bioelectron.* **2015**, *67*, 154.

[23] X. Zhu, Y. Qiao, X. Zhang, S. Zhang, X. Yin, J. Gu, Y. Chen, Z. Zhu, M. Li, Y. Shao, *Anal. Chem.* **2014**, *86*, 7001.

[24] D. W. M. Arrigan, *Analyst* **2004**, *129*, 1157.

[25] Y. Wang, J.-M. Noël, J. Velmurugan, W. Nogala, M. V. Mirkin, C. Lu, M. Guille Collignon, F. Lemaître, C. Amatore, *Proc. Natl. Acad. Sci. USA* **2012**, *109*, 11534.

[26] S. M. D. Watson, H. D. A. Mohamed, B. R. Horrocks, A. Houlton, *Nanoscale* **2013**, *5*, 5349.

[27] M. Schwartzkopf, G. Santoro, C. J. Brett, A. Rothkirch, O. Polonskyi, A. Hinz, E. Metwalli, Y. Yao, T. Strunskus, F. Faupel, P. Müller-Buschbaum, S. V. Roth, *ACS Appl. Mater. Interfaces* **2015**, *7*, 13547.

[28] M. Schwartzkopf, A. Hinz, O. Polonskyi, T. Strunskus, F. C. Lö, V. Kö, P. Mü Ller-Buschbaum, F. Faupel, S. V Roth, F. C. Löhrer, V. Körstgens,

P. Müller-Buschbaum, F. Faupel, S. V. Roth, *ACS Appl. Mater. Interfaces* **2017**, *9*, 5629.

[29] C. S. Smith, C. M. Bowie, K. D. Song, H. Yoon, V. K. Varadan, W. K. Kim, *Proc. SPIE* **2011**, *7980*, 798011.

[30] R. B. Morris, D. J. Franta, H. S. White, *J. Phys. Chem.* **1987**, *91*, 3559.

[31] A. J. Bard, L. R. Faulkner, *Electrochemical Methods: Fundamentals and Applications*, Wiley, New York **1980**.

[32] H. L. Woodvine, J. G. Terry, A. J. Walton, A. R. Mount, *Analyst* **2010**, *135*, 1058.

[33] K. Ngamchuea, S. Eloul, K. Tschulik, R. G. Compton, *J. Solid State Electrochem.* **2014**, *18*, 3251.

[34] E. J. F. Dickinson, R. G. Compton, *J. Phys. Chem. C* **2009**, *113*, 17585.

[35] I. Schmueser, A. J. Walton, J. G. Terry, H. L. Woodvine, N. J. Freeman, A. R. Mount, *Faraday Discuss.* **2013**, *164*, 295.

[36] C. L. Alexander, B. Tribollet, M. E. Orazem, *Electrochim. Acta* **2015**, *173*, 416.

[37] E. F. Douglass Jr., P. F. Driscoll, D. Liu, N. A. Burnham, C. R. Lambert, W. G. McGimpsey, *Anal. Chem.* **2008**, *80*, 7670.

[38] P. Sun, M. V. Mirkin, *Anal. Chem.* **2006**, *78*, 6526.

[39] X. M. Bin, E. H. Sargent, S. O. Kelley, *Anal. Chem.* **2010**, *82*, 5928.

[40] R. Gasparac, B. J. Taft, M. A. Lapierre-Devlin, A. D. Lazareck, J. M. Xu, S. O. Kelley, *J. Am. Chem. Soc.* **2004**, *126*, 12270.

[41] I. Ciani, H. Schulze, D. K. Corrigan, G. Henihan, G. Giraud, J. G. Terry, A. J. Walton, R. Pethig, P. Ghazal, J. Crain, C. J. Campbell, T. T. Bachmann, A. R. Mount, *Biosens. Bioelectron.* **2012**, *31*, 413.

[42] A. P. Wettasinghe, N. Singh, C. L. Starcher, C. C. DiTusa, Z. Ishak-Boushaki, D. Kahanda, R. McMullen, E. A. Motea, J. D. Slinker, *ACS Sens.* **2021**, *6*, 2622.

[43] S. Yilmaz, *J. Semicond.* **2015**, *36*, 082001.

[44] G. Maroli, S. Boyeras, H. Giannetta, S. Pazos, J. Gak, A. R. Oliva, M. A. Volpe, P. M. Julian, F. Palumbo, *Frontiers in Electronics*, **2023** 3 https://doi.org/10.3389/felec.2022.1060197.